Reactions of Laser-Ablated Osmium and Ruthenium Atoms with Carbon Dioxide: Matrix Infrared Spectra and Density Functional Calculations on OMCO, O_2MCO, $OMCO^-$ (M = Os, Ru), $O_2Os(CO)_2$, and $OCRu(O_2)CO$

Binyong Liang and Lester Andrews*

Department of Chemistry, University of Virginia, P.O. Box 400319, Charlottesville, Virginia 22904-4319

Received: January 9, 2002

Laser-ablated Os and Ru atoms react with CO_2 molecules upon cocondensation in excess argon at 7 K and neon at 4 K. Besides the dominant neutral products [OMCO, O_2MCO (M = Os, Ru), $O_2Os(CO)_2$, and $OCRu(O_2)CO$], anionic species [$OMCO^-$ (M = Os, Ru)] are also formed and identified through annealing, ultraviolet irradiation, isotopic substitution, and CCl_4-doping experiments. DFT calculations have been performed on possible products, and the overall agreement between the calculated and observed vibrational absorptions supports the product identifications.

I. Introduction

Carbon dioxide is a naturally abundant carbon source on the earth and hence a potential alternative precursor in organic synthesis. CO_2 is also a very stable triatomic molecule, and a significant amount of energy input is required for its activation and conversion. Transition metal complex catalysts, however, can reduce this activation energy substantially, and CO_2 fixation has become an important subject of research in organometallic and catalytic surface chemistry for many years.[1−5] The coordination of CO_2 with a metallic center is the key step in the CO_2 reduction, but the intermediate species formed during these reactions are still unknown.

Many research groups have studied transition metal atoms reacting with CO_2 by theoretical calculations and various spectroscopic methods. Theoretical calculations on first-row transition metal atoms[6−8] and cations[9,10] interacting with CO_2 have been reported, and different coordinated compounds have been found for early and late transition metals. By the use of thermal atom evaporation, complexes with first-row transition metals Ti through Cu have been studied in solid CO_2 matrixes.[11] Recent investigations of the reactions between laser-ablated metal atoms and CO_2 have revealed ionic in addition to neutral products.[12−17] The OMCO insertion product dominates these reactions for M = Sc to Ni. Previous studies[12,16,17] with Nb, Ta, Mo, W, and Re suggest that early second and third row metals are more reactive in this insertion reaction.

Ruthenium complexes, especially hydrides, have been extensively used in the catalytic reduction of CO_2,[3,18−20] whereas only a few examples could be found for osmium counterparts.[21] Two recent theoretical papers studied the intermediates and transition states in the ruthenium-catalyzed hydrogenation of CO_2.[22,23] It is important to study the intermediates in the direct reactions between Ru, Os, and CO_2, and this work may underscore the difference in the catalytic reduction of CO_2 with Ru and Os complexes.

In this paper, we present a study of laser-ablated ruthenium and osmium atoms reacting with CO_2 molecules in neon and argon matrixes. The products are identified by means of matrix infrared spectroscopy coupled with isotopic substitution experiments. Density functional theory (DFT) calculations are performed on proposed products to support the spectroscopic assignments and to provide more information on the reaction products.

II. Experimental and Computational Methods

The experimental methods for laser-ablation and matrix-isolation have been described in detail previously.[24−26] Briefly, the Nd:YAG laser fundamental (1064 nm, 10 Hz repetition rate with 10 ns pulse width, 3−10 mJ/pulse) was focused to ablate rotating ruthenium (Johnson-Matthey) or osmium (E-Vac Products) targets. Laser-ablated metal atoms were codeposited with carbon dioxide (0.2%-0.8%) in excess neon or argon onto a 4 K (neon) or 7 K (argon) CsI cryogenic window at 2−4 mmol/h for 0.5−1.5 h. Carbon dioxide (Matheson), isotopic $^{13}C^{16}O_2$ (Cambridge Isotopic Laboratories), 85% ^{18}O-enriched CO_2 (Spectra Gases), and selected mixtures were used in different experiments. Infrared spectra were recorded at 0.5 cm^{-1} resolution on a Nicolet 750 (neon work) or Nicolet 550 (argon work) spectrometer with 0.1 cm^{-1} accuracy using a mercury cadmium telluride detector down to 400 cm^{-1}. Matrix samples were annealed at different temperatures, and selected samples were subjected to photolysis using a medium-pressure mercury lamp with the globe removed ($\lambda > 240$ nm) and optical filters.

DFT calculations were performed on the proposed reaction products using the Gaussian 98 program[27] and the hybrid B3LYP[28] functional. The 6-311+G* basis set was used for carbon and oxygen,[29] and the LanL2DZ effective core potential and basis set was employed for ruthenium and osmium.[30] Such calculations helped to identify products in earlier transition metal−CO_2 reactions.[13−17]

III. Results

Infrared Spectra. Figures 1−4 show selected regions of the infrared spectra of reaction products of osmium and CO_2 in argon, and the bands and their isotopic counterparts are listed in the Table 1. Figure 5 shows the infrared spectra of the reaction product of Os + CO_2 in neon, and bands are listed in the Table 2. Figure 6 shows the 2160−1760 and 940−740 cm^{-1} infrared region of the reaction products between ruthenium and 0.5% CO_2 in argon, and Figures 7 and 8 show the neon matrix infrared

10.1021/jp0200167 CCC: $22.00
Published on Web 03/30/2002

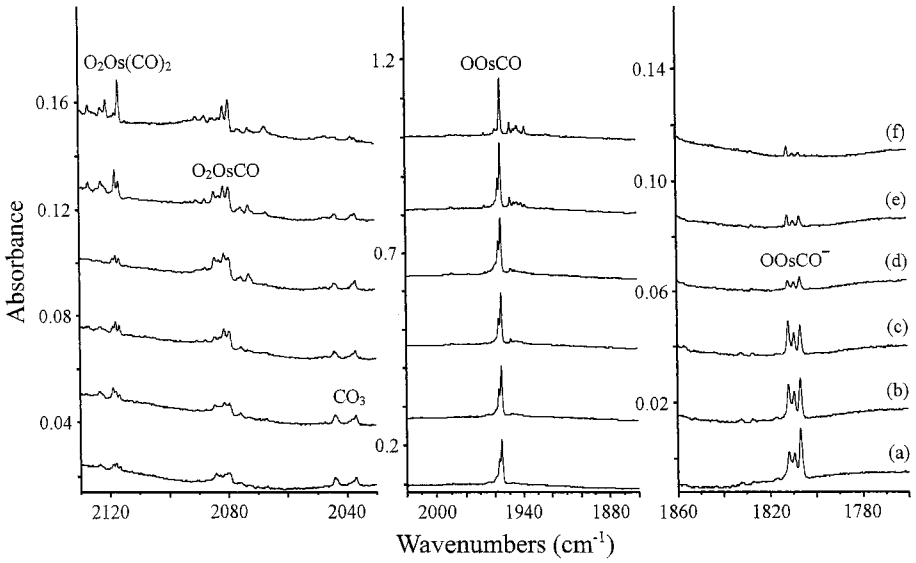

Figure 1. Infrared spectra in the 2130−1760 cm^{-1} region for laser-ablated Os codeposited with 0.5% CO_2 in argon at 7 K: (a) sample deposited for 70 min; (b) after 25 K annealing; (c) after $\lambda > 290$ nm irradiation; (d) after $\lambda > 240$ nm irradiation; (e) after 35 K annealing; (f) after 40 K annealing.

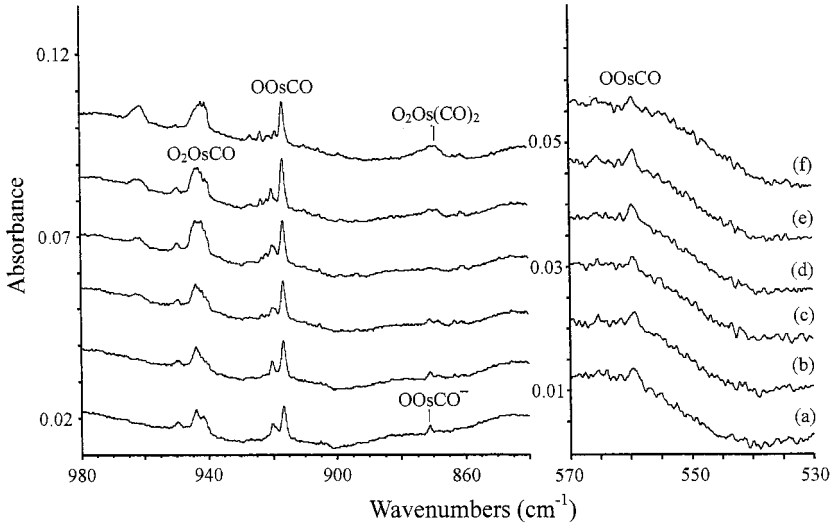

Figure 2. Infrared spectra in the 980−840 and 570−530 cm^{-1} regions. Spectra (a)−(f) are recorded with the same conditions as those in Figure 1.

spectra. Ruthenium-dependent argon and neon matrix infrared absorptions are listed in Tables 3 and 4, respectively, along with their isotopic counterparts. No new absorptions were observed in the regions of the CO_2 fundamentals, and spectra in these regions are not illustrated. Metal-independent bands, including CO_3, $C_2O_4^-$, and CO_2^-, listed in the osmium tables only, have been reported elsewhere[31−34] and will not be discussed in this paper.

DFT Calculations. The ground states for Os and Ru atoms were calculated as ^5D ($5d^6 6s^2$) and ^5F ($4d^7 5s^1$), respectively. Structures for all proposed product molecules were optimized, and analytical second-derivatives were used to obtain the harmonic frequencies. Calculations were done on different spin multiplicities for all molecules, and occupied and virtual orbitals were switched to confirm that the state under consideration was in fact the ground state. Different starting geometries were also used in the calculations: starting symmetry groups included C_{2v}, two different C_s, and C_1 for O_2RuCO. The calculation results are summarized in Tables 5, 6, and S7 (Supporting Information). Unrestricted DFT was used for open-shell systems and $\langle S^2 \rangle$ values after annihilation are listed; restricted DFT was employed for closed-shell molecules. The same ground states were found for corresponding osmium and ruthenium compounds, except for OMCO, for which the osmium species has the $^1A'$ ground state and the ruthenium analogue has the $^3A''$ ground state.

IV. Discussion

The behaviors of metal-dependent bands in different experiments will be described, and absorptions will be assigned to new metal + CO_2 products.

OOsCO. In the reaction of osmium atoms with CO_2 during condensation in the argon matrix, a strong band was observed at 1955.3 cm^{-1}. This band increased slightly on 25 K annealing (20%) and on irradiation (10%) and finally decreased on 40 K annealing (Figure 1). The 1955.3 cm^{-1} band in the carbonyl stretching region shifted to 1908.4 and to 1914.8 cm^{-1} in the $^{13}CO_2$ and $C^{18}O_2$ isotopic experiments, with carbon-12/13 and oxygen-16/18 isotopic ratios of 1.0246 and 1.0212, respectively. The larger carbon shift and smaller oxygen shift compared to the isolated CO molecule in the argon matrix reveal that the carbon atom in this C−O unit is bonded to another heavy atom.

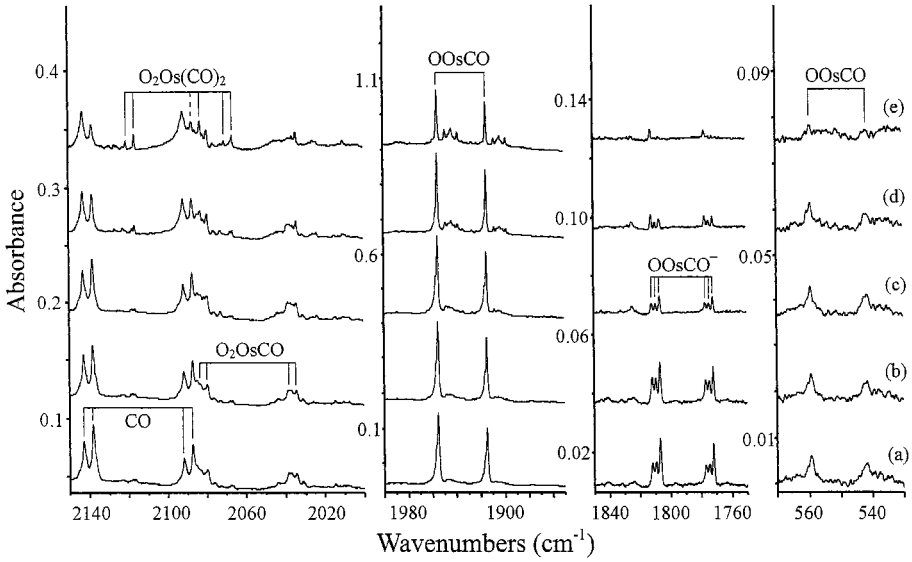

Figure 3. Infrared spectra in the 2150−1750 and 570−530 cm^{-1} regions for laser-ablated Os codeposited with 0.55% $C^{16}O_2$ + 0.45% $C^{18}O_2$ in argon at 7 K: (a) sample deposited for 100 min; (b) after 25 K annealing; (c) after λ > 240 nm irradiation; (d) after 35 K annealing; (e) after 40 K annealing.

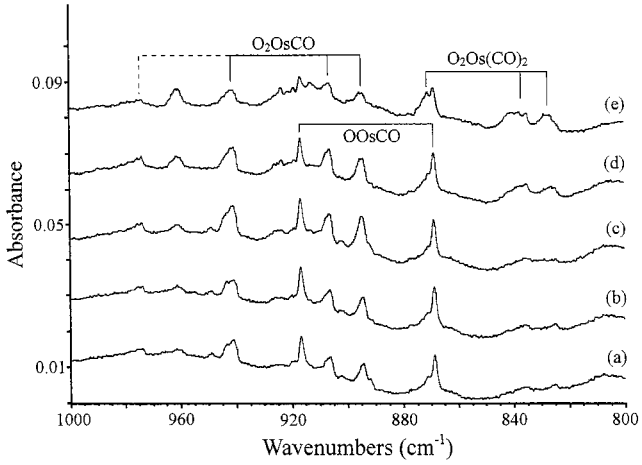

Figure 4. Infrared spectra in the 1000−800 cm^{-1} region for laser-ablated Os codeposited with 1% $C^{16}O_2$ + 1% $C^{18}O_2$ in argon at 7 K: (a) sample deposited for 90 min; (b) after 25 K annealing; (c) after λ > 240 nm irradiation; (d) after 35 K annealing; (e) after 40 K annealing.

In both mixed $^{12}C^{16}O_2$ + $^{13}C^{16}O_2$ and mixed $^{12}C^{16}O_2$ + $^{12}C^{18}O_2$ experiments, only doublets with two pure isotopic bands were found. Both results suggest that there is only one CO molecule involved in this carbonyl stretching mode. Another band at 916.7 cm^{-1} tracked with the 1955.3 cm^{-1} band in all experiments with only $^1/_{15}$ of the absorption intensity. This band only showed a miniscule 0.2 cm^{-1} shift with $^{13}CO_2$ but red-shifted to 868.7 cm^{-1} in the $C^{18}O_2$ experiment. This $^{16}O/^{18}O$ isotopic frequency ratio of 1.0553 is very close to the diatomic $Os^{16}O/Os^{18}O$ harmonic frequency ratio of 1.0557, which denotes an Os−O stretching mode. A third band at 559.6 cm^{-1} tracked with both the 1955.3 and 916.7 cm^{-1} absorptions, and this weak band only accounts for $^1/_{60}$ of the absorption intensity of the 1955.3 cm^{-1} band. The band was too weak to be observed in the $^{13}CO_2$ experiment but shifted to 541.7 cm^{-1} in the $C^{18}O_2$ experiment, and only doublets were observed in the mixed $C^{16}O_2$ + $C^{18}O_2$ experiment. On the basis of the aforementioned three bands, the OOsCO molecule is identified, and the absorptions at 1955.3, 916.7, and 559.6 cm^{-1} are assigned to the C−O stretching, Os−O stretching, and predominantly Os−CO stretching modes, respectively, on the basis of calculated displacement coordinates. In the neon matrix, only two modes were observed for this OOsCO molecule. The C−O and Os−O stretching modes at 1977.1 and 931.7 cm^{-1} are blue-shifted from the argon counterparts by 21.8 and 15.0 cm^{-1}, respectively. The former may be compared with OsCO at 1972.6 cm^{-1} in solid neon.[26] Isotopic shifts and mixed isotopic splitting patterns are very similar to their argon matrix counterparts, except that the Os−O stretching mode at 931.7 cm^{-1} was *blue-shifted* to 932.8 cm^{-1} in the $^{13}CO_2$ experiment. Although the exact reason for this unusual carbon-13 blue shift is unknown, on the basis of the limited experimental data, it is probably due to a Fermi resonance in which the overtone of a lower mode interacts with

TABLE 1: Infrared Absorptions (cm^{-1}) from Reaction of Laser-Ablated Os Atoms with CO_2 in Excess Argon at 7 K

$^{12}C^{16}O_2$	$^{13}C^{16}O_2$	$^{12}C^{18}O_2$	*R*(12/13)	*R*(16/18)	assignment
2344.8	2279.2	2309.7	1.0288	1.0152	CO_2
2339.0	2273.6	2304.1	1.0288	1.0152	CO_2
2143.0	2095.8	2092.0	1.0225	1.0244	$(CO)_x$
2138.3	2091.1	2087.2	1.0226	1.0245	CO
2120.9	2074.1	2070.5	1.0226	1.0243	$O_2Os(CO)_2$ site
2116.7	2070.0	2066.4	1.0226	1.0243	$O_2Os(CO)_2$
2084.5	2036.2	2039.1	1.0237	1.0223	O_2OsCO site
2079.7	2031.1	2034.3	1.0239	1.0223	O_2OsCO
2043.9	1990.0		1.0271		CO_3 site
2037.0	1983.3	2007.3	1.0271	1.0148	CO_3
2025.9					
1955.3	1908.4	1914.8	1.0246	1.0212	OOsCO
1948.5	1901.7	1908.2	1.0246	1.0211	OOsCO site
1943.3	1896.5	1903.3	1.0247	1.0210	OOsCO site
1938.0	1891.2	1898.4	1.0247	1.0209	OOsCO site
1856.8	1806.5	1826.7	1.0275	1.0161	$C_2O_4^-$
1811.9	1767.2	1777.0	1.0253	1.0196	$OOsCO^-$ site
1809.5	1764.6	1774.5	1.0254	1.0197	$OOsCO^-$ site
1806.8	1761.9	1771.9	1.0255	1.0197	$OOsCO^-$
1383.9	1368.3	1339.2	1.0114	1.0334	$(CO_2)_x$
1279.0	1255.9	1227.7	1.0184	1.0418	$(CO_2)_x$
960.7		913.3		1.0519	O_2OsX?
949.2		902.1		1.0522	OsO_2
940.8	940.7	894.3		1.0520	O_2OsCO
916.7	916.5	868.7		1.0553	OOsCO
871.0		825.2		1.0555	$OOsCO^-$
868.2	868.1	825.0		1.0524	$O_2Os(CO)_2$
663.5	644.6	653.5	1.0293	1.0153	CO_2
661.9	643.2	651.9	1.0291	1.0153	CO_2
559.6		541.7		1.0330	OOsCO

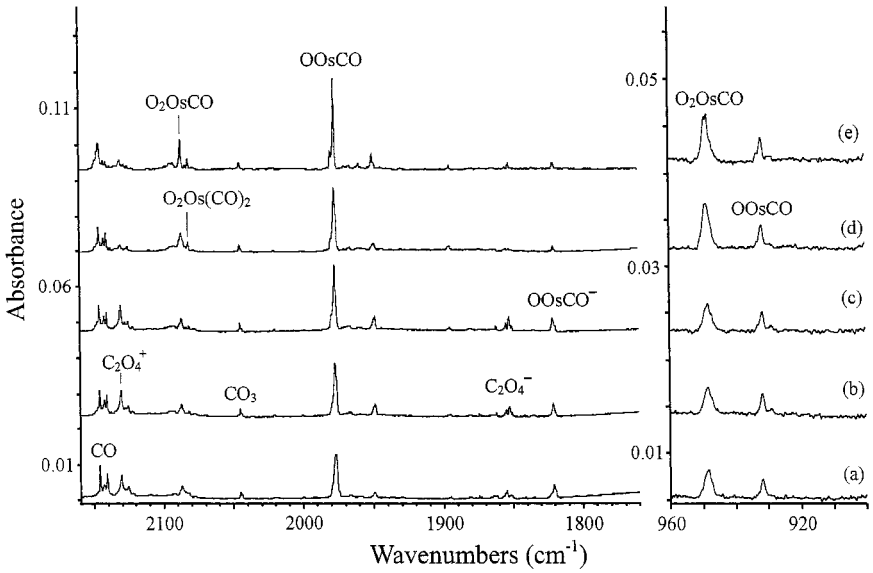

Figure 5. Infrared spectra in the 2160−1760 and 960−900 cm^{-1} regions for laser-ablated Os codeposited with 0.2% CO_2 in neon at 4 K: (a) sample deposited for 30 min; (b) after 8 K annealing; (c) after 10 K annealing; (d) after $\lambda > 240$ nm irradiation; (e) after 12 K annealing.

TABLE 2: Infrared Absorptions (cm^{-1}) from Reaction of Laser-Ablated Os Atoms with CO_2 in Excess Neon at 4 K

$^{12}C^{16}O_2$	$^{13}C^{16}O_2$	$^{12}C^{18}O_2$	*R*(12/13)	*R*(16/18)	assignment
2347.6	2281.8	2312.5	1.0288	1.0152	CO_2
2146.1	2098.8	2095.1	1.0225	1.0243	$(CO)_x$
2142.6	2095.4	2091.5	1.0225	1.0244	$(CO)_x$
2140.8	2093.7	2089.8	1.0225	1.0244	CO
2130.8	2074.5		1.0271		$C_2O_4^+$
2086.7	2038.3	2041.4	1.0238	1.0223	O_2OsCO
2081.7	2035.7	2032.3	1.0226	1.0243	$O_2Os(CO)_2$
2044.9	1991.1		1.0270		CO_3
2020.3					
1977.1	1930.0	1935.7	1.0244	1.0214	OOsCO
1948.7	1901.8	1908.7	1.0247	1.0210	OOsCO site
1862.0	1812.0				$C_2O_4^-$ site
1854.9					$C_2O_4^-$ site
1852.4	1802.9	1823.1	1.0275	1.0161	$C_2O_4^-$
1850.8	1801.0	1820.8	1.0277	1.0165	$C_2O_4^-$ site
1820.9	1775.8	1785.7	1.0254	1.0197	$OOsCO^-$
1747.9	1703.7	1714.3	1.0259	1.0196	$XOsCO^-$
1670.1	1625.6	1642.3	1.0274	1.0169	$(CO_2)_2CO_2^-$
1665.3	1621.0	1637.6	1.0273	1.0169	$(CO_2)CO_2^-$
1658.2	1614.0	1630.5	1.0274	1.0170	CO_2^-
1421.6	1380.2	1399.6	1.0300	1.0157	CO_2^+
1387.7	1369.7	1346.6	1.0131	1.0305	$(CO_2)_x$
1284.3	1264.6	1229.6	1.0156	1.0445	$(CO_2)_x$
1274.4	1263.0	1227.5	1.0090	1.0382	$C_2O_4^+$
1256.4	1247.5		1.0071		CO_4^-
1189.2	1181.4		1.0066		$C_2O_4^-$
965.6	965.2	914.3		1.0561	
948.4	948.4	901.4		1.0521	O_2OsCO
931.7	932.8	883.3		1.0548	OOsCO
897.4	897.1	853.6		1.0513	$O_2Os(CO)_2$
668.2	649.1	658.3	1.0294	1.0150	CO_2

this Os−O vibration and the neon matrix has positioned the carbon-12 overtone band above and the carbon-13 overtone band below the Os−O stretching fundamental. A similar anomaly was observed for OMnNCO, but such coincidences are uncommon.[35]

The B3LYP calculation predicted the ground electronic state of OOsCO as $^1A'$, while the lowest triplet $^3A''$ and quintet $^5A''$ states are 5.4 and 18.8 kcal/mol higher, respectively. For the ground $^1A'$ state, the C−O stretching, the Os−O stretching, and the Os−CO stretching modes are predicted at 2052.5, 994.2, and 584.4 cm^{-1} with intensities of 1004, 84, and 16 km/mol, respectively. The calculated vibrational frequencies and their relative intensities matched the experimental data very well. The calculated isotopic frequencies also predict carbon-12/13 and oxygen-16/18 ratios for the C−O stretching mode as 1.0250 and 1.0213, respectively, while the observed ratios are 1.0244 and 1.0214. Excellent agreement of isotopic ratios for Os−O and Os−CO stretching modes are also obtained. The unobserved predominantly Os−C−O bending mode calculated at 507.7 cm^{-1} probably provides the overtone band for the unusual carbon-13 blue shift described above. This fundamental, calculated at 507.7 cm^{-1} with a 15.9 cm^{-1} ^{13}C-shift, probably gives rise to ^{12}C and ^{13}C overtone positions near 950 and 920 cm^{-1}, respectively, and hence, the vibrational interaction forces the Os−O mode down with ^{12}C and up with ^{13}C. Finally, OOsCO is formed in the direct insertion of Os into the CO_2 molecule, reaction 1, which is exothermic by 26.3 kcal/mol on the basis of the B3LYP calculation.

$$Os + CO_2 \rightarrow OOsCO \qquad (\Delta E = -26.3 \text{ kcal/mol}) \quad (1)$$

No new absorption was observed in the regions of the CO_2 fundamentals that might be due to unreacted Os−OCO complexes. This includes the Fermi doublet where sharp, weak 1383.9 and 1279.0 cm^{-1} bands due to $(CO_2)_x$ were observed in solid argon,[13−15] and any Os−OCO formed might be expected to give additional absorption, but none was observed. As reaction 1 suggests, such weak complexes are much higher in energy. The implication here is that all Os and CO_2 encounters result in reaction 1, and the growth on 25 K annealing (Figure 1) suggests that reaction 1 is spontaneous. We cannot, of course, detect Os−OCO complexes if their absorptions are common to strong absorptions of CO_2 itself.

ORuCO. In the reaction of ruthenium with CO_2, a strong, broad absorption was observed at 1966.1 cm^{-1} on deposition in the argon matrix. The band failed to change following annealing but increased by 60% on full mercury lamp irradiation. Two more associated bands were observed at 836.1 and 509.0 cm^{-1}, and their isotopic counterparts are listed in Table 3. Note that only doublets were observed in both mixed $^{12}CO_2 + {}^{13}CO_2$ and mixed $C^{16}O_2 + C^{18}O_2$ experiments. Similar to the OOsCO molecule discussed above, the three bands at 1966.1, 836.1, and 509.0 cm^{-1} are assigned to the C−O stretching, Ru−O stretching, and primarily Ru−CO stretching modes in

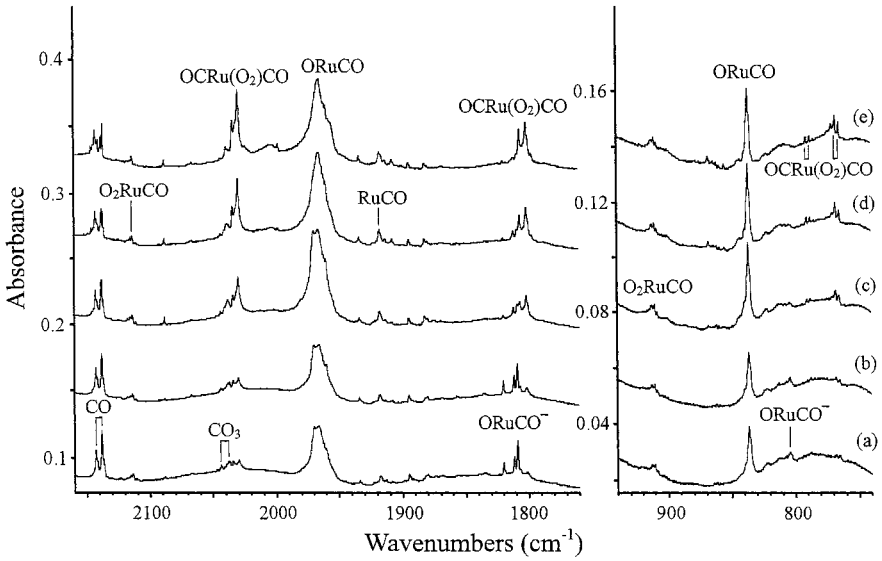

Figure 6. Infrared spectra in the 2160−1760 and 940−740 cm^{-1} regions for laser-ablated Ru codeposited with 0.5% CO_2 in argon at 7 K: (a) sample deposited for 60 min; (b) after 25 K annealing; (c) after $\lambda > 240$ nm irradiation; (d) after 35 K annealing; (e) after 40 K annealing.

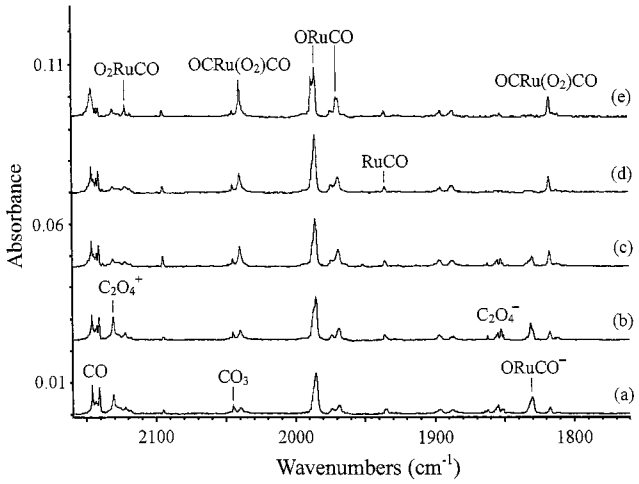

Figure 7. Infrared spectra in the 2160−1760 cm^{-1} region for laser-ablated Ru codeposited with 0.2% CO_2 in neon at 4 K: (a) sample deposited for 30 min; (b) after 8 K annealing; (c) after $\lambda > 290$ nm irradiation; (d) after $\lambda > 240$ nm irradiation; (e) after 12 K annealing.

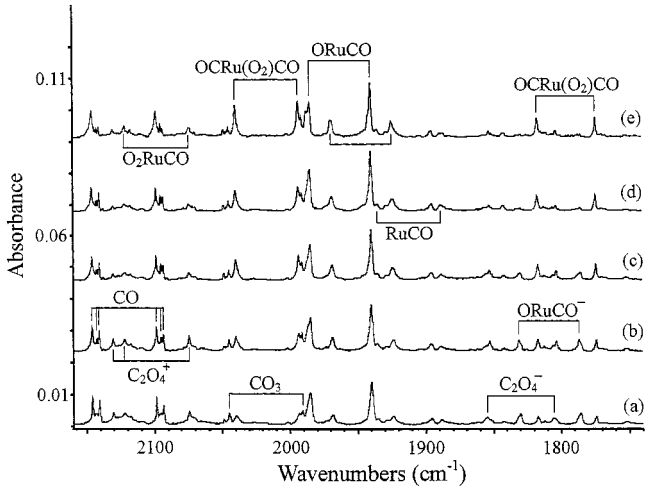

Figure 8. Infrared spectra in the 2160−1740 cm^{-1} region for laser-ablated Ru codeposited with 0.15% $^{12}CO_2$ + 0.15% $^{13}CO_2$ in neon at 4 K: (a) sample deposited for 40 min; (b) after 8 K annealing; (c) after $\lambda > 290$ nm irradiation; (d) after $\lambda > 240$ nm irradiation; (e) after 12 K annealing.

the ORuCO molecule, respectively. In the neon matrix, the same molecule was also identified, the C−O mode was blue-shifted to 1984.8 cm^{-1}, and the Ru−O mode was shifted to 847.2 cm^{-1}. Both bands showed similar annealing and ultraviolet irradiation behavior, and similar isotopic splitting patterns compared to their argon matrix counterparts. The only difference is that the C−O stretching absorption is sharper in the neon matrix with less matrix interaction. The simple RuCO carbonyl was observed lower at 1917.7 and 1935.6 cm^{-1} in solid argon and neon, respectively.[26]

DFT calculations on ORuCO were performed for three different multiplicities. The lowest states for each multiplicity are listed in Table 6. In contrast to OOsCO, the most stable state found is $^3A''$, while $^1A'$ and $^5A''$ states are only 9.5 and 10.2 kcal/mol higher. For the ground $^3A''$ state, the vibrational analysis predicts C−O stretching, Ru−O stretching, and Ru−CO stretching modes at 2068.2, 856.5, and 496.0 cm^{-1}, which are in good agreement with both neon and argon matrix values. The isotopic frequencies for these three modes are also calculated and listed in Table S7 (Supporting Information), and they show consistent agreement with the experimental values. The energy of ORuCO is lower than that of Ru atom and CO_2 molecule by only 1.8 kcal/mol, and hence Ru is less reactive than Os with CO_2. Nevertheless, we failed to find evidence for any Ru−OCO complexes. On photolysis, substantial reaction occurred; this is probably due to diffusion and reaction of Ru and CO_2 under irradiation.

O_2OsCO. The weak, broad band at 2079.7 cm^{-1} observed in the Os + CO_2/Ar matrix increased on early annealing and irradiation and sharpened on final annealing to 40 K. This band shifted to 2031.1 and 2034.3 cm^{-1} in the $^{13}CO_2$ and $C^{18}O_2$ experiments, with carbon-12/13 and oxygen-16/18 isotopic frequency ratios of 1.0239 and 1.0223, respectively. In both mixed $^{12}CO_2$ + $^{13}CO_2$ and mixed $C^{16}O_2$ + $C^{18}O_2$ isotopic experiments, only doublets with pure isotopic bands were observed. It is clear that this band is due to the vibration of a single carbonyl. In the Os−O stretching region, a band at 940.8 cm^{-1} tracked with the 2079.7 cm^{-1} band with almost the same absorption intensity in all experiments. This band showed miniscule isotopic shift with $^{13}CO_2$ but shifted to 894.3 cm^{-1} in the $C^{18}O_2$ experiment. The oxygen-16/18 isotopic frequency ratio of 1.0520 is considerably lower than the OsO diatomic harmonic ratio of 1.0557, but it is very close to the 16/18 ratio

TABLE 3: Infrared Absorptions (cm^{-1}) from Reaction of Laser-Ablated Ru Atoms with CO_2 in Excess Argon at 7 K

$^{12}C^{16}O_2$	$^{13}C^{16}O_2$	$^{12}C^{18}O_2$	*R*(12/13)	*R*(16/18)	assignment
2117.8	2069.9	2069.4	1.0231	1.0234	O_2RuCO site
2115.6	2067.6	2067.5	1.0232	1.0233	O_2RuCO site
2113.8	2065.8	2065.7	1.0232	1.0233	O_2RuCO
2088.4	2042.4	2038.6	1.0225	1.0244	
2033.0	1987.8	1988.4	1.0227	1.0224	$OCRu(O_2)CO$ site
2029.8	1983.7	1984.3	1.0232	1.0229	$OCRu(O_2)CO$
1966.1	1920.1	1921.8	1.0240	1.0231	ORuCO
1959.8	1915.3	1915.7	1.0232	1.0230	ORuCO site
1917.6	1872.3	1877.3	1.0242	1.0215	RuCO
1820.2	1776.0	1783.5	1.0249	1.0206	$ORuCO^-$ site
1811.4	1767.3	1775.2	1.0250	1.0204	$ORuCO^-$ site
1808.7	1764.6	1772.6	1.0250	1.0204	$ORuCO^-$
1806.3	1764.0	1769.0	1.0240	1.0211	$OCRu(O_2)CO$ site
1801.0	1759.4	1763.6	1.0236	1.0212	$OCRu(O_2)CO$
1102.6	1084.5	1065.0	1.0167	1.0353	$OCRu(O_2)CO$
912.9	912.9	872.9		1.0458	$O_2{}^{99}RuCO$
912.0	911.9	871.9		1.0460	$O_2{}^{100}RuCO$
911.0	910.9	870.9		1.0460	$O_2{}^{101}RuCO$
910.1	910.1	870.0		1.0461	$O_2{}^{102}RuCO$
908.3	908.1	868.0		1.0464	$O_2{}^{104}RuCO$
902.1	902.1	862.8			RuO_2
867.6		830.1		1.0452	$OCRu(O_2)CO$
836.1	834.7	794.9		1.0518	ORuCO
804.1	804.1	764.8		1.0514	$ORuCO^-$
790.4		781.3		1.0116	$OCRu(O_2)CO$
787.3		778.3		1.0116	$OCRu(O_2)CO$ site
767.2	763.7	729.2		1.0521	$OCRu(O_2)CO$
764.5	760.6	726.9		1.0517	$OCRu(O_2)CO$ site
509.0		495.8		1.0266	ORuCO

TABLE 4: Infrared Absorptions (cm^{-1}) from Reaction of Laser-Ablated Ru Atoms with CO_2 in Excess Neon at 4 K

$^{12}C^{16}O_2$	$^{13}C^{16}O_2$	$^{12}C^{18}O_2$	*R*(12/13)	*R*(16/18)	assignment
2121.6	2073.6	2073.3	1.0231	1.0233	O_2RuCO
2117.8	2069.8	2069.6	1.0232	1.0233	O_2RuCO site
2094.9	2048.9	2045.2	1.0225	1.0243	
2039.8	1993.2	1993.9	1.0234	1.0230	$OCRu(O_2)CO$
1984.8	1939.5	1941.5	1.0234	1.0223	ORuCO
1968.4	1924.0	1925.3	1.0231	1.0224	ORuCO site
1935.4	1889.5	1894.9	1.0243	1.0214	RuCO
1896.7					
1830.8	1786.5	1793.8	1.0248	1.0206	$ORuCO^-$
1816.7	1773.7	1775.5	1.0242	1.0232	$OCRu(O_2)CO$
1752.5	1708.9	1719.6	1.0255	1.0191	$XRuCO^-$
1087.1					$OCRu(O_2)CO$
922.0	922.0	881.3		1.0462	$O_2{}^{99}RuCO$
921.0	920.8	880.3		1.0462	$O_2{}^{100}RuCO$
919.1	918.9	878.3		1.0465	$O_2{}^{102}RuCO$
917.2	917.0	876.5		1.0464	$O_2{}^{104}RuCO$
867.1					$OCRu(O_2)CO$
849.8	848.6	808.2		1.0515	ORuCO site
848.3	847.4	806.8		1.0514	ORuCO site
847.2	846.1	805.2		1.0522	ORuCO
771.6	768.2	733.5		1.0519	$OCRu(O_2)CO$

for the ν_3 mode of the OsO_2 molecule (1.0524).[36] In the mixed $C^{16}O_2 + C^{18}O_2$ experiment, two more bands were observed at 906.4 and 973.9 cm^{-1}, besides the pure isotopic bands. The 940.8 cm^{-1} band is appropriate for a O−Os−O antisymmetric stretching mode, and the extra bands at 906.4 and 973.9 cm^{-1} in the mixed $C^{16}O_2 + C^{18}O_2$ experiment are the antisymmetric and symmetric stretching vibrations of the $^{16}O-Os-^{18}O$ unit. The O_2OsCO molecule is hence identified, and bands at 2079.7 and 940.8 cm^{-1} are due to the C−O stretching and O−Os−O antisymmetric stretching modes. In the neon matrix, the same two modes of the O_2OsCO molecule were observed at 2086.7 and 948.4 cm^{-1}, blue-shifted from the argon counterparts by 7.0 and 7.6 cm^{-1}, respectively. Similar isotopic frequency ratios and splitting patterns in the mixed isotopic experiments were also observed.

DFT calculation on O_2OsCO predicted the ground state as $^1A_1$ for this planar molecule with C_{2v} symmetry (Table 5). The lowest triplet and quintet states are 20.8 and 83.7 kcal/mol higher, respectively. The vibrational analysis on the $^1A_1$ ground state revealed the C−O and antisymmetric O−Os−O stretching modes at 2161.9 and 989.1 cm^{-1}, with intensities of 617 and 262 km/mol, respectively. These two modes require scale factors of 0.965 and 0.959, respectively, which are typical values for B3LYP calculations; however, the calculation underestimated the infrared intensities of the antisymmetric O−Os−O mode. The calculated isotopic frequency ratios are also in excellent agreement with the observed values. Calculations were also performed on another isomer, $Os(O_2)CO$, in which two oxygen atoms bridge between osmium and carbon atoms. The two lowest states are found to be $^3B_2$ and $^3A_2$, and they are 53.9 and 62.3 kcal/mol, respectively, higher than the $^1A_1$ ground-state O_2OsCO (Table 5). In the current system, the most probable oxygen source is CO_2, and reaction 2 is the likely pathway.

$$CO_2 + OOsCO \rightarrow O_2OsCO + CO \quad (\Delta E = +2.3 \text{ kcal/mol}) \quad (2)$$

Although this reaction is endothermic by 2.3 kcal/mol in the current B3LYP calculation, reaction during sample deposition could be activated by the energized product of reaction 1. However, growth during annealing requires an exothermic reaction. The observed O_2OsCO could be produced via the exothermic reactions of osmium oxide with CO_2 or O atom with OOsCO. The presence of O atoms is manifested by the observation of CO and CO_3 and OsO by the detection of OsO_2.[32,36]

O_2RuCO. In the argon matrix, the new band at 2113.8 cm^{-1} is weak on deposition, but it increased by half on full-arc irradiation and decreased slightly on annealing to 40 K. In the $^{13}CO_2$ and $C^{18}O_2$ experiments, this band shifted to 2065.8 and 2065.7 cm^{-1}, with carbon-12/13 and oxygen-16/18 isotopic frequency ratios of 1.0232 and 1.0233, respectively. In both mixed $^{12}CO_2 + {}^{13}CO_2$ and mixed $C^{16}O_2 + C^{18}O_2$ experiments, only doublets with pure isotopic bands were observed. This band is assigned to the C−O stretching mode of the O_2RuCO molecule in the argon matrix, and two nearby bands at 2115.6 and 2117.8 cm^{-1} with similar behavior in all experiments are due to bands of the same molecule at different matrix sites. The antisymmetric O−Ru−O stretching mode of O_2RuCO is also observed, and more importantly, the ruthenium natural isotopic splitting pattern is resolved. The bands at 912.9, 912.0, 911.0, 910.1, and 908.3 cm^{-1} are due to the antisymmetric O−Ru−O stretching mode in $O_2{}^nRuCO$ where *n*, the mass number of ruthenium, equals 99, 100, 101, 102, and 104, respectively. The intensity profile of these five bands reflects the natural abundance of ruthenium isotopes and hence affirms that the molecule is a single-metal species. The isotopic counterparts of these bands are listed in the Table 3, and the average oxygen-16/18 ratio of 1.0461 is close to the same value of ν_3 mode in the RuO_2 molecule (1.0454). In the mixed $C^{16}O_2 + C^{18}O_2$ experiment, two additional broad bands were observed at 921.5 and 873.7 cm^{-1}; however, no ruthenium isotopic structure could be resolved. If in the O_2RuCO molecule, one assumes that the O−Ru−O antisymmetric stretching mode does not involve the CO subunit (this is valid because no isotopic shift was observed in the $^{13}CO_2$ experiment), the frequencies of apex and terminal isotopic molecule pairs can be used to

TABLE 5: Equilibrium Geometry and Frequencies Calculated for Products in the Reaction of Osmium and CO_2[a]

species[b]		geometry[c]	frequencies, cm^{-1} (intensity, km/mol)
OOsCO	$^1A'$ (C_s) (0)	O−Os, 1.696; Os−C, 1.838; C−O, 1.156; ∠OOsC, 109.0; ∠OsCO, 170.1	181.1 (11), 453.8 (0), 507.7 (5), 584.4 (16), 994.2 (84), 2052.5 (1004)
	$^3A''$ (C_s) (+5.4) ⟨2.0002⟩	O−Os, 1.739; Os−C, 1.865; C−O, 1.156; ∠OOsC, 116.1; ∠OsCO, 168.3	155.7 (20), 445.9 (0), 485.1 (1), 557.9 (14), 866.6 (155), 2040.6 (1049)
	$^5A''$ (C_s) (+18.8) ⟨6.0000⟩	O−Os, 1.766; Os−C, 1.989; C−O, 1.146; ∠OOsC, 151.5; ∠OsCO, 169.7	75.2 (12), 398.8 (2), 431.0 (2), 432.5 (12), 851.1 (105), 2067.7 (902)
O_2OsCO	$^1A_1$ (C_{2v}) (0)	O−Os, 1.707; Os−C, 1.934; C−O, 1.136; ∠OOsO, 136.9	126.5 (0), 190.2 (3), 238.1 (8), 395.4 (6), 484.2 (10), 510.1 (7), 989.1 (262), 1031.0 (16), 2161.9 (617)
	$^3A''$ (C_s) (+20.8) ⟨2.0001⟩	O−Os, 1.744; Os−C, 1.887; C−O, 1.146; ∠OOsO, 124.2; ∠OOsC, 108.6; ∠OsCO, 174.1	112.4 (0), 172.3 (12), 229.4 (11), 322.3 (3), 475.1 (4), 545.7 (13), 876.3 (128), 927.6 (45), 2091.9 (941)
$Os(O_2)CO'$	$^3B_2$ (C_{2v}) (+53.9) ⟨2.0001⟩	Os−O, 1.934; O−C, 1.375; C−O′, 1.183; ∠OOsO, 67.9; ∠OCO′, 128.3	173.3 (1), 443.8 (22), 449.0 (3), 671.3 (3), 773.7 (19), 799.6 (101), 914.6 (26), 1012.9 (117), 1895.3 (667)
	$^3A_2$ (C_{2v}) (+62.3) ⟨2.0001⟩	Os−O, 1.974; O−C, 1.365; C−O′, 1.189; ∠OOsO, 66.1; ∠OCO′, 127.9	177.5 (1), 360.7 (0), 423.7 (25), 611.8 (0), 780.9 (48), 793.9 (27), 929.5 (51), 1011.1 (146), 1866.3 (704)
$O_2Os(CO)_2$	^1A_g (D_{2h}) (0)	O−Os, 1.751; Os−C, 2.047; C−O, 1.127	29.7 (2), 78.0 (0), 108.0 (2), 145.4 (0), 190.1 (4), 287.8 (53), 348.1 (0), 407.9 (0), 446.7 (0), 486.4 (11), 494.2 (8), 872.9 (271), 952.4 (0), 2187.9 (1267), 2249.9 (0)
	$^1A_1$ (C_{2v}) (+12.3)	O−Os, 1.766; Os−C, 1.918; C−O, 1.142; ∠OOsO, 109.0; ∠COsC, 102.3; ∠OsCO, 173.5; ∠OOsC, 111.4	75.0 (10), 100.4 (0), 119.3 (0), 154.8 (49), 268.5 (6), 286.5 (4), 394.3 (0), 420.8 (13), 495.9 (1), 589.4 (19), 511.2 (84), 828.8 (201), 896.4 (52), 2027.5 (2505), 2147.1 (406)
$OCOs(O_2)C'O'$	$^3A''$ (C_s) (+4.9) ⟨2.0002⟩	O−C, 1.148; C−Os, 1.896; Os−O(1), 1.914; Os−O(2), 2.090; O−C′(1), 1.447; O−C′(2), 1.309; C′−O′, 1.186; ∠OOsO, 66.0	14.4i (5), 93.3 (3), 157.5 (2), 377.7 (21), 413.9 (7), 455.1 (3), 514.7 (17), 570.2 (3), 618.7 (15), 764.4 (136), 784.4 (23), 828.1 (55), 1122.8 (92), 1889.1 (772), 2091.4 (955)
$OOsCO^-$	$^2A''$ (C_s) (0) ⟨0.7501⟩	O−Os, 1.754; Os−C, 1.819; C−O, 1.186; ∠OOsC, 116.4; ∠OsCO, 167.6	171.1 (8), 473.1 (0), 507.3 (2), 604.9 (5), 882.8 (135), 1878.2 (1362)
	$^2A'$ (C_s) (+11.8) ⟨0.7502⟩	O−Os, 1.762; Os−C, 1.846; C−O, 1.186; ∠OOsC, 127.1; ∠OsCO, 164.6	149.5 (7), 470.4 (1), 495.4 (9), 580.0 (2), 857.2 (196), 1868.3 (1242)
O_2OsCO^-	$^2B_2$ (C_{2v}) (0) ⟨0.7500⟩	O−Os, 1.758; Os−C, 1.845; C−O, 1.182; ∠OOsO, 136.8	135.0 (4), 140.7 (0), 238.9 (2), 260.1 (2), 493.1 (5), 588.0 (3), 884.5 (334), 901.0 (115), 1919.8 (915)
	$^2A_2$ (C_{2v}) (+24.1) ⟨0.7501⟩	O−Os, 1.770; Os−C, 1.917; C−O, 1.164; ∠OOsO, 122.5	102.5 (2), 212.8 (2), 230.9 (6), 352.3 (0), 525.4 (0), 559.3 (24), 831.5 (340), 904.3 (41), 1997.6 (873)

[a] DFT calculation: B3LYP functional, 6-311+G* basis set on C and O, LANL2DZ basis set and ECP on Os. [b] Two or three electronic states are listed for each species, labels in the first parentheses denote point groups, numbers in the second parentheses denote the relative energies (kcal/mol) compared to the ground states, and the last entry for open-shell molecules is $\langle S^2 \rangle$ after annihilation. [c] Bond lengths are given in Å; bond angles are given in degrees.

deduce the O−Ru−O bond angle.[37,38] On the basis of the five pairs of terminal isotopic molecules, the upper limit O−Ru−O bond angle is determined as 148° ± 2°, and on the basis of the apex isotopic molecules, the lower limit is 130° ± 3°. In the neon matrix, the C−O stretching mode of the O_2RuCO molecule was observed at 2121.6 cm^{-1}, which is blue-shifted 7.8 cm^{-1} from the argon matrix value. For the antisymmetric O−Ru−O stretching mode, four isotopic bands were resolved as listed in the Table 4. Similarly, the upper limit of the O−Ru−O bond angle in the neon matrix is determined as 144° ± 2°, and the lower limit is 131° ± 4°.

In the DFT calculations, the ground state of the O_2RuCO molecule is predicted as $^1A_1$, possessing C_{2v} symmetry. The C_s symmetry $^1A'$ state is 38.7 kcal/mol higher, whereas the lowest triplet state, $^3A''$, is 8.8 kcal/mol higher. The bond angle of ORuO in the ground $^1A_1$ state is 141.8°, which is between of the limits of the angle deduced from both neon and argon matrix infrared absorptions. Two strong bands, the C−O stretching and antisymmetric O−Ru−O stretching modes, are predicted at 2190.0 and 966.2 cm^{-1}, and their isotopic frequency ratios are listed in Table S7 (Supporting Information). These calculated frequencies are in very good agreement with the spectroscopic observations. The calculations on another isomer, $Ru(O_2)CO$, are quite different from their Os counterparts. Two lowest states of $Ru(O_2)CO$, $^3A_2$ and $^3B_2$, have almost the same energy and are 5.5 and 5.4 kcal/mol, respectively, lower than the $^1A_1$ state

TABLE 6: Equilibrium Geometry and Frequencies Calculated for Products in the Reaction of Ruthenium and CO_2[a]

species [b]		geometry[c]	frequencies, cm^{-1} (intensity, km/mol)
ORuCO	$^3A''$ (C_s) (0) ⟨2.0002⟩	O−Ru, 1.731; Ru−C, 1.882; C−O, 1.147; ∠ORuC, 106.8; ∠RuCO, 167.5	137.8 (14), 381.6 (1), 429.6 (2), 496.0 (13), 856.5 (104), 2068.2 (804)
	$^1A'$ (C_s) (+9.5)	O−Ru, 1.716; Ru−C, 1.852; C−O, 1.148; ∠ORuC, 100.5; ∠RuCO, 173.2	166.4 (9), 390.8 (0), 482.7 (11), 524.2 (13), 901.8 (101), 2074.0 (895)
	$^5A''$ (C_s) (+10.2) ⟨6.0000⟩	O−Ru, 1.782; Ru−C, 2.105; C−O, 1.134; ∠ORuC, 169.3; ∠RuCO, 175.5	60.3 (13), 320.8 (25), 327.8 (0), 336.7 (0), 783.2 (40), 2144.0 (877)
O_2RuCO	$^1A_1$ (C_{2v}) (0)	O−Ru, 1.698; Ru−C, 2.004; C−O, 1.130; ∠ORuO, 141.8	94.6 (1), 158.8 (7), 240.7 (14), 259.2 (0), 381.1 (2), 403.6 (5), 966.2 (341), 969.8 (13), 2190.0 (529)
	$^3A''$ (C_s) (+8.8) ⟨2.0001⟩	O−Ru, 1.745; Ru−C, 1.934; C−O, 1.135; ∠ORuO, 126.6; ∠ORuC, 105.0; ∠RuCO, 173.4	109.7 (0), 157.3 (20), 239.3 (10), 354.0 (5), 406.9 (0), 454.9 (14), 833.6 (127), 883.2 (17), 2146.4 (752)
$Ru(O_2)CO'$	$^3A_2$ (C_{2v}) (−5.5) ⟨2.0001⟩	Ru−O, 1.981; O−C, 1.353; C−O′, 1.194; ∠ORuO, 65.9; ∠OCO′, 127.2	206.1 (73), 340.0 (2), 422.8 (19), 625.5 (0), 751.6 (33), 905.9 (1357), 949.3 (25), 1047.8 (151), 1834.7 (582)
	$^3B_2$ (C_{2v}) (−5.4) ⟨2.0001⟩	Ru−O, 1.964; O−C, 1.358; C−O′, 1.191; ∠ORuO, 67.1; ∠OCO′, 126.9	176.4 (19), 370.7 (10), 422.6 (22), 636.0 (3), 765.6 (45), 848.9 (426), 937.2 (21), 1043.4 (120), 1846.3 (515)
$OCRu(O_2)C'O'$	$^3A''$ (C_s) (0) ⟨2.0002⟩	O−C, 1.139; C−Ru, 1.953; Ru−O(1), 1.919; Ru−O(2), 2.494; O−C′(1), 1.420; O−C′(2), 1.309; C′−O′, 1.191; ∠ORuO, 66.2	79.9 (2), 86.4 (3), 159.9 (2), 356.9 (7), 384.3 (29), 420.8 (0), 448.8 (3), 531.6 (1), 625.4 (3), 752.4 (84), 793.3 (23), 841.1 (66), 1126.5 (101), 1853.2 (672), 2125.5 (847)
	$^3A_2$ (C_{2v}) (+13.9) ⟨2.0004⟩	O−C, 1.131; C−Ru, 2.103; Ru−O, 2.001; O−C′, 1.343; C′−O′, 1.195; ∠ORuO, 64.2; ∠OC′O′, 121.9	249.5i (21), 40.8 (4), 128.8 (0), 175.5 (1), 307.8 (33), 344.5 (1), 360.0 (9), 404.6 (0), 638.0 (5), 720.6 (29), 805.8 (21), 978.0 (1), 1098.4 (126), 1809.6 (544), 2165.6 (961)
	$^3A'$ (C_s) (+18.3) ⟨2.0003⟩	O−C, 1.133; C−Ru, 2.047; Ru−O(1), 2.021; Ru−O(2), 2.027; O−C′(1), 1.349; O−C′(2), 1.332; C′−O′, 1.197; ∠ORuO, 64.3	50.2 (4), 73.2 (1), 175.0 (2), 295.7 (2), 334.7 (23), 353.5 (5), 402.6 (0), 519.2 (9), 625.5 (4), 713.7 (24), 810.7 (52), 964.9 (5), 1100.5 (117), 1798.1 (477), 2151.7 (855)
	$^1A'$ (C_s) (+20.4)	O−C, 1.140; C−Ru, 1.924; Ru−O(1), 1.835; Ru−O(2), 2.109; O−C′(1), 1.544; O−C′(2), 1.274; C′−O′, 1.182; ∠ORuO, 68.3	93.8 (2), 114.5 (0), 145.9 (1), 306.2 (45), 372.6 (120), 402.5 (10), 476.0 (11), 483.5 (2), 551.8 (4), 729.0 (128), 763.3 (23), 811.8 (25), 1178.9 (88), 1936.0 (731), 2121.9 (800)
$O_2Ru(CO)_2$	$^1A_1$ (C_{2v}) (+39.4)	O−Ru, 1.733; Ru−C, 2.117; C−O, 1.125; ∠ORuO, 162.9; ∠CRuC, 172.5; ∠RuCO, 179.4; ∠ORuC, 90.6	49.4 (1), 65.5 (0), 117.4 (0), 157.1 (7), 194.4 (9), 240.5 (15), 281.8 (6), 302.3 (0), 382.0 (0), 388.1 (3), 408.4 (12), 908.5 (4), 920.1 (310), 2207.3 (921), 2241.1 (6)
	^1A_g (D_{2h}) (+39.8)	O−Ru, 1.737; Ru−C, 2.118; C−O, 1.125	97.7i (8), 61.7 (0), 66.7 (0), 121.8 (0), 163.4 (9), 237.8 (24), 275.6 (0), 301.8 (0), 379.0 (3), 390.4 (0), 415.2 (13), 905.9 (0), 910.0 (324), 2211.2 (888), 2246.0 (0)
	$^1A_1$ (C_{2v}) (+49.1)	O−Ru, 1.759; Ru−C, 1.941; C−O, 1.135; ∠ORuO, 112.3; ∠CRuC, 103.6; ∠RuCO, 174.1; ∠ORuC, 110.1	15.1i (13), 92.5 (0), 107.5 (51), 114.7 (0), 246.5 (4), 260.7 (5), 357.2 (4), 386.8 (0), 431.2 (0), 474.8 (60), 552.2 (25), 814.2 (236), 888.4 (34), 2083.9 (1795), 2172.6 (374)
$ORuCO^-$	$^2A''$ (C_s) (0) ⟨0.7503⟩	O−Ru, 1.769; Ru−C, 1.814; C−O, 1.178; ∠ORuC, 108.7; ∠RuCO, 170.0	150.0 (8), 412.8 (1), 474.3 (13), 569.7 (7), 814.6 (174), 1894.3 (1450)
	$^4A''$ (C_s) (+3.6) ⟨3.7501⟩	O−Ru, 1.803; Ru−C, 1.887; C−O, 1.180; ∠ORuC, 134.3; ∠RuCO, 160.5	136.0 (13), 415.2 (1), 447.5 (0), 533.3 (3), 754.6 (225), 1866.7 (1229)
	$^2A'$ (C_s) (+11.9) ⟨0.7506⟩	O−Ru, 1.795; Ru−C, 1.845; C−O, 1.181; ∠ORuC, 119.6; ∠RuCO, 167.5	132.6 (12), 412.8 (2), 422.7 (9), 542.3 (6), 753.0 (239), 1869.9 (1392)

[a] DFT calculation: B3LYP functional, 6-311+G* basis set on C and O, LANL2DZ basis set and ECP on Ru. [b] Two or more electronic states are listed for each species, labels in the first parentheses denote point groups, numbers in the second parentheses denote the relative energies (kcal/mol) compared to the ground states, and the last entry for open-shell molecules is $\langle S^2 \rangle$ after annihilation. [c] Bond lengths are given in Å; bond angles are given in degrees.

O_2RuCO (Table 6). Vibrational analysis on the $^3A_2$ state of $Ru(O_2)CO$ predicted a carbonyl stretching mode at 1834.7 cm^{-1} with an infrared intensity of 582 km/mol and a very strong mixed mode at 905.9 cm^{-1} with an intensity of 1357 km/mol. No bands in these regions can be assigned to these two modes. Two possible reasons for not observing this lower energy isomer come to mind. First, DFT energy calculations on transition metal molecules are not absolutely accurate, and the 5.5 kcal/mol energy difference is within in the uncertainty range. Second, the formation of $Ru(O_2)CO$ in the current reaction is kinetically unfavorable, and isomerization from O_2RuCO is unlikely. Analogous to O_2OsCO, the reaction of CO_2 and ORuCO is endothermic (33.9 kcal/mol), and the O_2RuCO molecule observed in the matrix experiment is probably produced by the ruthenium oxide reaction with CO_2 or the O atom combination with ORuCO.

$$O + ORuCO \rightarrow O_2RuCO \qquad (3)$$

$O_2Os(CO)_2$. In the argon matrix, the band at 2116.7 cm^{-1} was weak after deposition. It increased slightly on annealing to 25 K, showed little change on irradiation, but increased markedly on annealing to 35 and 40 K. In the $^{13}CO_2$ and $C^{18}O_2$ experiments, the band red-shifted to 2070.0 and 2066.4 cm^{-1} with isotopic frequency ratios of 1.0226 and 1.0243, respectively. In the mixed $^{12}CO_2 + {}^{13}CO_2$ experiment, an intermediate band was observed at 2084.7 cm^{-1} in addition to the two pure isotopic bands. A similar intermediate band was observed at 2083.1 cm^{-1} in the mixed $C^{16}O_2 + C^{18}O_2$ experiment. This band must be assigned to an antisymmetric C−O stretching mode in a dicarbonyl unit. In the Os−O stretching region, a broad band at 868.2 cm^{-1} tracked with the 2116.7 cm^{-1} band. This band red-shifted to 825.0 cm^{-1} with $C^{18}O_2$, and the oxygen-16/18 isotopic frequency ratio of 1.0524 is close to the ratio for the antisymmetric O−Os−O stretching in the O_2OsCO molecule. The triplet feature with a new band at 835.0 cm^{-1} in the mixed $C^{16}O_2 + C^{18}O_2$ experiment characterizes an O−Os−O stretching mode. Overall, the molecule $O_2Os(CO)_2$ is identified, and bands at 2116.7 and 868.2 cm^{-1} are the antisymmetric C−O and O−Os−O stretching modes, respectively. In the neon matrix, the $O_2Os(CO)_2$ molecule absorbed at 2081.7 and 897.4 cm^{-1}, and both bands showed similar matrix shifts and splitting patterns in the isotopic experiments as their argon counterparts.

DFT calculation on this $O_2Os(CO)_2$ molecule predicted the ground state as ^1A_g, which is a planar molecule with D_{2h} symmetry. For C_{2v} symmetry, in which O_2Os and $Os(CO)_2$ are in two perpendicular planes, higher energy singlet and triplet states converged. The frequency analysis on the ^1A_g state predicted antisymmetric Os−O and C−O stretching modes at 872.9 and 2187.9 cm^{-1}, with infrared intensities of 271 and 1267 km/mol, respectively, which are in excellent agreement with the observed spectrum. The isotopic frequency ratios, listed in Table S7 (Supporting Information), are also in excellent agreement with the experimental results. In contrast, the C_{2v} singlet state, which is 12.3 kcal/mol higher, has frequencies at 2027.5 and 828.8 cm^{-1}. These are lower than the observed bands, and the relative calculated intensities are 12:1, which are not compatible with experiment. This molecule is probably formed via reaction 4, which is exothermic by 5.5 kcal/mol in the DFT calculation.

$$OOsCO + CO_2 \rightarrow O_2Os(CO)_2 \qquad (\Delta E = -5.5 \text{ kcal/mol}) \qquad (4)$$

In light of the $OCRu(O_2)CO$ molecule to be discussed in the next paragraph, calculations on $OCOs(O_2)CO$ were performed. The lowest state is $^3A''$, which is 4.9 kcal/mol higher in energy than the ^1A_g ground state of $O_2Os(CO)_2$ (Table 5).

$OCRu(O_2)CO$. In the Ru + CO_2 argon matrix experiment, two weak bands at 2029.8 and 1801.0 cm^{-1} increased slightly on annealing to 25 K, almost tripled on full-arc irradiation, and increased markedly after the 35 and 40 K annealings (Figure 6). In the experiments with varying conditions, different CO_2 concentrations and laser powers, these two bands tracked with each other throughout the annealing and irradiation cycles with fixed relative intensities (4:3). In the $^{13}CO_2$ and $C^{18}O_2$ experiments, both bands showed appropriate isotopic shifts for carbonyl stretching modes, as listed in Table 3. In both mixed $^{12}CO_2 + {}^{13}CO_2$ and mixed $C^{16}O_2 + C^{18}O_2$ isotopic experiments, only doublets with pure isotopic absorptions were observed for both bands. It is clear that bands at 2029.8 and 1801.0 cm^{-1} are due to two isolated single carbonyl stretching modes in one molecule; the upper band is likely due to a terminal and the lower to a bridging carbonyl. Four more weaker associated bands were observed at 1102.6, 867.6, 790.4, and 767.2 cm^{-1}. In the $^{13}CO_2$ experiment, the isotopic counterparts of the comparatively stronger 1102.6 and 767.2 bands were observed at 1084.5 and 763.7 cm^{-1}, whereas no isotopic counterparts could be identified for the two weaker 867.6 and 790.4 cm^{-1} bands. In the $C^{18}O_2$ experiments, isotopic counterparts were observed for all four bands, as listed in Table 3. Based on the absorption frequencies and isotopic frequency ratios, both 867.6 and 767.2 cm^{-1} bands are approximately Ru−O stretching modes and the 1102.6 and 790.4 cm^{-1} bands are mixed modes. The molecule $OCRu(O_2)CO$ is proposed, in which two middle oxygen atoms form bridges between ruthenium and carbon atoms. The same molecule was also observed in the neon matrix, and five modes are found at 2039.8, 1816.7, 1087.1, 867.1, and 771.6 cm^{-1}. The isotopic counterparts are listed in the Table 4.

DFT calculation revealed $OCRu(O_2)CO$ to be a very interesting molecule. The initial trial started at C_{2v} symmetry, with all atoms in one plane, and OCRu···CO on the C_2 axis. Both singlet and triplet states were converged, and the triplet $^3A_2$ state is 29.1 kcal/mol lower in energy than the $^1A_1$ state. However, both states have a large imaginary frequency for deviation of atoms from the C_2 axis, indicating that they are transition states. Calculations then were performed in C_s symmetry, and the lowest state was found as $^3A''$, whereas the lowest singlet state $^1A'$ and another triplet state $^3A'$ are 20.4 and 18.5 kcal/mol higher, respectively. This $^3A''$ state is also 13.9 kcal/mol lower than the C_{2v} symmetry $^3A_2$ state, and more importantly, no imaginary vibrational frequencies were found. The geometry of this ground state is depicted in Figure 9, and it is obvious that the molecule actually is an adduct of ORuCO and CO_2 in which CO_2 adds across the Ru−O bond in a [2+2] cycloaddition reaction. It should also be noted that the ground state of $OCRu(O_2)CO$ is $^3A''$, in accord with the $^3A''$ ground state of ORuCO. From the DFT calculation, the addition reaction is exothermic by 10.4 kcal/mol.

$$ORuCO + CO_2 \rightarrow OCRu(O_2)CO \qquad (\Delta E = -10.4 \text{ kcal/mol}) \qquad (5)$$

The vibrational analysis predicted six modes at 2125.5, 1853.2, 1126.5, 841.1, 793.3, and 752.4 cm^{-1}, with infrared intensities of 847, 672, 101, 66, 23, and 84 km/mol, respectively. These results agree with the experimental data very well. Calculated isotopic frequency ratios are listed in Table S7 (Supporting Information), and again they showed very good agreement with the experimental values. From the calculation, the two mixed

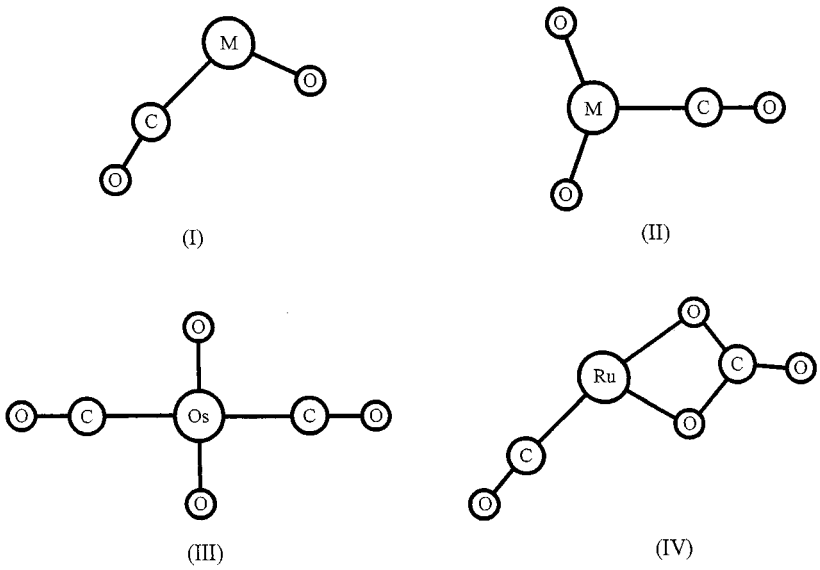

Figure 9. Structures for observed species: (I) OMCO and $OMCO^-$ (M = Os, Ru); (II) O_2MCO (M = Os, Ru); (III) $O_2Os(CO)_2$; (IV) $OCRu(O_2)CO$.

modes observed in the argon matrix at 1102.6 and 790.4 cm^{-1} are approximately symmetric OCO stretching and out-of-plane CO_3 bending modes.

A more conventional metal + $2CO_2$ complex, $O_2Ru(CO)_2$, was not observed in both neon and argon matrixes, which suggests that this isomer is higher in energy than the $OCRu(O_2)CO$ molecule. DFT calculation on $O_2Ru(CO)_2$ was first performed in D_{2h} symmetry; however, an imaginary frequency was found at 97.7 cm^{-1} for this ^1A_g state. Slight bending of the molecule lowered the total energy 0.4 kcal/mol for this $^1A_1$ state and eliminated the imaginary mode. Calculations were also performed for three other input geometries and a triplet spin state, and all converged states are higher in energy than the $^1A_1$ ground state (Table 6). This $^1A_1$ state, however, is still 39.4 kcal/mol higher in energy than the $^3A''$ ground state of $OCRu(O_2)CO$, which justifies the lack of $O_2Ru(CO)_2$ molecule in these experiments.

$OOsCO^-$. In the reaction between Os and CO_2 in the argon matrix, a three-band-set at 1811.9, 1809.5, and 1806.8 cm^{-1} was observed on deposition; these bands are 10-fold weaker than the OOsCO absorptions (Figure 1). The overall absorption intensity of this band set showed little change on early annealing, increased slightly on $\lambda > 470$ nm irradiation, decreased slightly on $\lambda > 290$ nm irradiation, then decreased 80% on $\lambda > 240$ nm irradiation, and did not regain the absorption intensity in the following annealing (Figure 1). This band set was red-shifted to 1767.2, 1764.6, and 1761.9 cm^{-1} and 1777.0, 1774.5, and 1771.9 cm^{-1} in the $^{13}CO_2$ and $C^{18}O_2$ experiments, with average carbon-12/13 and oxygen-16/18 isotopic frequency ratios of 1.0254 and 1.0197, respectively, which signifies a strong M−C and C−O interaction, much like that observed for $OsCO^-$ at 1785.5 cm^{-1}.[26] In both mixed $^{12}CO_2 + {}^{13}CO_2$ and mixed $C^{16}O_2 + C^{18}O_2$ experiments, only pure isotopic bands were observed, which demonstrated that only one carbon atom and one oxygen atom are involved in this vibrational mode. The band is still in the carbonyl stretching region with typical carbonyl isotopic shifts, but the comparatively lower wavenumber indicates a weaker interaction between carbon and oxygen atoms. This three-band set is assigned to the C−O stretching mode of the $OOsCO^-$ anion in three argon matrix sites. The much weaker Os−O stretching mode of this anion was identified at 871.0 cm^{-1} with only $^1/_{20}$ of the absorption intensity of the carbonyl stretching mode. In the $C^{18}O_2$ experiment, this band shifted to 825.2 cm^{-1}; the oxygen-16/18 isotopic ratio of 1.0555 is very close to the diatomic harmonic value of 1.0557. In the mixed $C^{16}O_2 + C^{18}O_2$ experiment, no intermediate bands were found.

Additional experiments were performed using 0.05% CCl_4 as an additive in the reagent gas while keeping other conditions the same, and this C−O stretching band is almost eliminated, whereas the weaker Os−O band is not observed. CCl_4 is well-known for its high electron capture cross-section, and most ablated electrons are captured by CCl_4 instead of product molecules. Hence, the anion assignment is supported by the CCl_4-doped experiments.[39−43] In the neon matrix, only the C−O stretching mode of this $OOsCO^-$ anion was observed at 1820.9 cm^{-1}. The neon matrix value is blue-shifted from the argon matrix value by 14.1 cm^{-1}, and carbon 12/13 and oxygen 16/18 isotopic ratios of 1.0254 and 1.0197 are almost identical to their argon counterparts. Similar to the argon matrix, this neon matrix band is completely eliminated in the CCl_4-doped experiment.

DFT calculation predicts a ground state $^2A''$ for the $OOsCO^-$ anion. The quartet state calculation did not converge, and intermediate results showed much higher energy. The calculation on the $^2A''$ ground state predicts a strong C−O stretching mode at 1878.2 cm^{-1}, which requires a scale factor of 0.969 for the neon matrix band. This is 174.3 cm^{-1} lower than that predicted for OOsCO, and the $OOsCO^-$ band is observed 156.2 cm^{-1} lower than that of OOsCO in solid neon. Furthermore, the computed carbon-12/13 and oxygen-16/18 isotopic ratios (1.0258 and 1.0201) agree with the experiment very well. The Os−O mode is predicted at 882.8 cm^{-1}, with intensity of 135 km/mol, which is less than $^1/_{10}$ of the C−O stretching mode (1362 km/mol). This anion is produced via electron capture during the deposition process as laser ablation also provides electrons:

$$OOsCO + e^- \rightarrow OOsCO^- \qquad (\Delta E = -56.0 \text{ kcal/mol}) \tag{6}$$

The electron affinity for OOsCO is calculated as 56.0 kcal/mol, which is higher than calculated (33.3 kcal/mol) for OsCO.[26] The slight increase in $OOsCO^-$ absorption with $\lambda > 470$ nm irradiation comes at the expense of CO_2^- absorption in which this light photodetaches CO_2^- and these electrons are captured

by OOsCO. In this regard, the analogous OReCO$^-$ anion exhibits similar photobleaching and has almost the same computed electron affinity (55.7 kcal/mol).[42]

Photobleaching of OOsCO$^-$ begins at $\lambda > 290$ nm but is more efficient at $\lambda > 240$ nm. Photodestruction of matrix-isolated anions with mercury arc radiation typically requires higher energy photons than gas-phase photodetachment.[43] Similar experiments have found that 1−2 eV in excess of the gas-phase laser photodetachment threshold is necessary for photodestruction of $Ni(CO)_{1,2,3}^-$ in solid argon.[39] Hence, the DFT calculation is a better predictor of electron affinity than the matrix photochemistry in which matrix−anion interactions will affect the cross section and energy of photodetachment processes.

ORuCO$^-$. The analogous anion, ORuCO$^-$, was also observed in the Ru + CO_2/Ar experiment. The three-band set observed at 1820.2, 1811.4, and 1808.7 cm^{-1} on deposition showed little change on annealing to 25 K, almost disappeared on full-arc irradiation, and did not re-appear in the following annealings. This band set has ^{13}C and ^{18}O counterparts at 1776.0, 1767.3, and 1764.6 cm^{-1}, and 1783.5, 1775.2, and 1772.6 cm^{-1}, with the average isotopic ratio of 1.0250 and 1.0205, respectively. In both mixed isotopic experiments, only doublets with pure isotopic bands were found. In the 0.02% CCl_4-doped experiment, this band decreased more than $^3/_4$, which is diagnostic of an anion.[39−43] This three-band-set is assigned to the C−O stretching mode for the ORuCO$^-$ anion in three matrix sites. The weaker Ru−O stretching mode was observed at 804.1 cm^{-1}, and the oxygen-16/18 isotopic frequency ratio of 1.0514 is close to the same ratio in the ORuCO molecule. In the neon matrix, the carbonyl stretching mode of this anion was observed at 1830.8 cm^{-1}, which is blue-shifted from the argon matrix value by 22.1 cm^{-1}, and also increased slightly with $\lambda > 470$ nm irradiation. The isotopic counterparts and their ratios are listed in the Table 4. The RuCO$^-$ anion was observed slightly lower at 1792.8 and 1782.5 cm^{-1} in solid neon and argon, respectively.[26]

DFT calculation predicts the ground state of ORuCO$^-$ as ^{2}A″, whereas two other states, ^{4}A″ and ^{2}A′, also converged but are 3.6 and 11.9 kcal/mol higher. The vibrational analysis of the ^{2}A″ state predicts a C−O vibrational mode at 1894.3 cm^{-1} with an intensity of 1450 km/mol. This result requires a scale factor of 0.966 for the neon matrix value. Also predicted are the carbon-12/13 and oxygen-16/18 isotopic frequency ratios as 1.0249 and 1.0214, which are in good agreement with the experimental ratios of 1.0248 and 1.0206. The Ru−O mode is calculated at 814.6 cm^{-1}, with intensity of 174 km/mol, about $^1/_8$ of the C−O mode, and these results also agree well with our experimental observations. Finally, the electron affinity of ORuCO is calculated as 45.8 kcal/mol, which is higher than calculated (28.5 kcal/mol) for RuCO.[26]

Other Absorptions. In the osmium and CO_2 experiment in the neon matrix, a very weak band at 1747.9 cm^{-1} showed appropriate isotopic shifts for a carbonyl anion stretching mode and split into doublets in the mixed isotopic experiments. Clearly, only one CO is involved. Similar to OOsCO$^-$ bands, this band was eliminated by full-arc photolysis and was not observed in the CCl_4-doped experiment. We have considered the possibility of the O_2OsCO^- anion; however, the DFT calculations (Table 5) do not support this assignment, and we only assign it generically as XOsCO$^-$. A similar band was also observed at 1752.5 cm^{-1} in the ruthenium and CO_2/Ne experiment, and again we assign it as XRuCO$^-$.

In the ruthenium and CO_2 experiments, a weak band at 1917.6 cm^{-1} in argon and at 1935.4 cm^{-1} in neon is due to the C−O stretching mode of RuCO. This molecule has been discussed in detail in an earlier report,[26] and the same isotopic shifts were observed in the current isotopic substitution experiments.

IV. Conclusions

Laser-ablated Os and Ru atoms react with CO_2 molecules upon cocondensation in excess argon at 7 K and neon at 4 K. Neutral products [OMCO, O_2MCO, (M = Os, Ru), $O_2Os(CO)_2$, and $OCRu(O_2)CO$], as well as anionic species [OMCO$^-$ (M = Os, Ru)], are identified through annealing, ultraviolet irradiation, and isotopic substitution experiments. Previous investigations with Fe and CO_2 in argon[14] gave the analogous major species OFeCO and OFeCO$^-$. Anionic assignments are further supported by CCl_4-doping experiments in which anions were not observed because of the high electron capture cross section of the CCl_4 additive.[39−41] DFT/B3LYP calculations have been performed on all products, and the overall agreement between the calculated and observed vibrational absorptions supports the product identifications.

The very favorable reaction between Os and CO_2 suggests that Os-centered complexes have the potential to be good catalysts for CO_2 reduction. It is noteworthy that the major reaction product, OOsCO, also inserts into the second CO_2 molecule and forms $O_2Os(CO)_2$. Although Ru is less reactive than Os in the insertion reaction with CO_2, the addition reaction between ORuCO and CO_2 to give $OCRu(O_2)CO$ is spontaneous, which suggests that XRuO complexes are good catalysts for CO_2 reduction.

The OMCO and OMCO$^-$ species may be compared with their MCO and MCO$^-$ analogues.[26] In every case, the latter carbonyl frequencies are lower indicating more π charge transfer from M to CO than from OM to CO. This effect is more pronounced for Fe[14] than for Ru than for Os neutrals but about the same for the three metal anion species. Finally, the insertion reactions have widely varying energy changes, +15.9, −1.8, and −26.3 kcal/mol for Fe, Ru, and Os, for which the OMCO ground states are ^{5}A″, ^{3}A″, and ^{1}A′, respectively. This trend justifies the spontaneous reaction of Os and CO_2 and the requirement of activation for the Fe and CO_2 reaction[14] and underscores the great stability of the osmium−oxygen bond.

Acknowledgment. We appreciate support from N.S.F. Grant CHE 00-78836.

Supporting Information Available: Table S7 containing calculated isotopic frequencies for vibrations observed in the matrix infrared experiments. This material is available free of charge via the Internet at http://pubs.acs.org.

References and Notes

(1) Palmer, D. A.; van Eldik, R. *Chem. Rev.* **1983**, *83*, 651.
(2) Culter, A. R.; Hanna, P. K.; Vites, J. C. *Chem. Rev.* **1988**, *88*, 1363.
(3) Jessop, P. G.; Ikariya, T.; Noyori, R. *Chem. Rev.* **1995**, *95*, 259.
(4) Gibson, D. H. *Chem. Rev.* **1996**, *96*, 2063.
(5) Gibson, D. H. *Coord. Chem. Rev.* **1999**, *185*−*186*, 335.
(6) Jeung, G. H. *Chem. Phys. Lett.* **1995**, *232*, 319.
(7) P·pai, I.; Mascetti, J.; Fournier, R. *J. Phys. Chem. A* **1997**, *101*, 4465.
(8) Mascetti, J.; Galan, F.; Pápai, I. *Coord. Chem. Rev.* **1999**, *190*−*192*, 557.
(9) Fan, H. J.; Liu, C. W. *Chem. Phys. Lett.* **1999**, *300*, 351.
(10) Sodupe, M.; Branchadell, V.; Rosi, M.; Bauschlicher, C. W., Jr. *J. Phys. Chem. A* **1997**, *101*, 7854.
(11) Mascetti, J.; Tranquille, M. *J. Phys. Chem.* **1988**, *92*, 2177.
(12) Souter, P. F.; Andrews, L. *Chem. Commun.* **1997**, 777. Souter, P. F.; Andrews, L. *J. Am. Chem. Soc.* **1997**, *119*, 7350 (Cr, Mo, W + CO_2).
(13) Zhou, M. F.; Andrews, L. *J. Am. Chem. Soc.* **1998**, *120*, 13230 (Sc + CO_2).

(14) Zhou, M. F.; Liang, B.; Andrews, L. *J. Phys. Chem. A* **1999**, *103*, 2013 (Cr, Mn, Fe, Co, Ni, Cu + CO_2).
(15) Zhou, M. F.; Andrews, L. *J. Phys. Chem. A* **1999**, *103*, 2066 (V, Ti + CO_2).
(16) Wang, X.; Chen, M.; Zhang, L.; Qin, Q. Z. *J. Phys. Chem. A* **2000**, *104*, 758 (Ta + CO_2).
(17) Chen, M.; Wang, X.; Zhang, L.; Qin, Q. Z. *J. Phys. Chem. A* **2000**, *104*, 7010 (Nb + CO_2).
(18) For example, see: (a) Jessop, P. G.; Ikariya, T.; Noyori, R. *Nature* **1994**, *368*, 231; *Science* **1995**, *269*, 1065. (b) Jessop, P. G.; Hsiao, Y.; Ikariya, T.; Noyori, R. *J. Am. Chem. Soc.* **1996**, *118*, 344. (c) Jessop, P. G.; Ikariya, T.; Noyori, R. *Chem. Rev.* **1999**, *99*, 475.
(19) Mizukawa, T.; Tsuge, K.; Nakajima, H.; Tanaka, K. *Angew. Chem., Int. Ed.* **1999**, *38*, 362.
(20) Laurenczy, G.; Joo, F.; Nadasdi, L. *Inorg. Chem.* **2000**, *39*, 5083.
(21) (a) Flood, T. C.; Lim, J. K.; Deming, M. A. *Organometallics* **2000**, *19*, 2310. (b) Chardon-Noblat, S.; Deronzier, A.; Hartl, F.; van Slageren, J.; Mahabiersing, T. *Eur. J. Inorg. Chem.* **2001**, 613.
(22) Musashi, Y.; Sakaki, S. *J. Am. Chem. Soc.* **2000**, *122*, 3867.
(23) Matsubara, T. *Organometallics* **2001**, *20*, 19.
(24) Burkholder, T. R.; Andrews, L. *J. Chem. Phys.* **1991**, *95*, 8697.
(25) Hassanzadeh, P.; Andrews, L. *J. Phys. Chem.* **1992**, *96*, 9177.
(26) Zhou, M. F.; Andrews, L. *J. Phys. Chem. A* **1999**, *103*, 6956.
(27) Frisch, M. J.; Trucks, G. W.; Schlegel, H. B.; Scuseria, G. E.; Robb, M. A.; Cheeseman, J. R.; Zakrzewski, V. G.; Montgomery, J. A., Jr.; Stratmann, R. E.; Burant, J. C.; Dapprich, S.; Millam, J. M.; Daniels, A. D.; Kudin, K. N.; Strain, M. C.; Farkas, O.; Tomasi, J.; Barone, V.; Cossi, M.; Cammi, R.; Mennucci, B.; Pomelli, C.; Adamo, C.; Clifford, S.; Ochterski, J.; Petersson, G. A.; Ayala, P. Y.; Cui, Q.; Morokuma, K.; Malick, D. K.; Rabuck, A. D.; Raghavachari, K.; Foresman, J. B.; Cioslowski, J.; Ortiz, J. V.; Stefanov, B. B.; Liu, G.; Liashenko, A.; Piskorz, P.; Komaromi, I.; Gomperts, R.; Martin, R. L.; Fox, D. J.; Keith, T.; Al-Laham, M. A.; Peng, C. Y.; Nanayakkara, A.; Gonzalez, C.; Challacombe, M.; Gill, P. M. W.; Johnson, B. G.; Chen, W.; Wong, M. W.; Andres, J. L.; Head-Gordon, M.; Replogle, E. S.; Pople, J. A. *Gaussian 98*, revision A.1; Gaussian, Inc.: Pittsburgh, PA, 1998.
(28) Lee, C.; Yang, E.; Parr, R. G. *Phys. Rev. B* **1988**, *37*, 785.
(29) McLean, A. D.; Chandler, G. S. *J. Chem. Phys.* **1980**, *72*, 5639. Wachters, A. J. H. *J. Chem. Phys.* **1970**, *52*, 1033. Hay, P. J. *J. Chem. Phys.* **1977**, *66*, 4377. K. Raghavachari, K.; Trucks, G. W. *J. Chem. Phys.* **1989**, *91*, 1062.
(30) Hay, P. J.; Wadt, W. R. *J. Chem. Phys.* **1985**, *82*, 270. Wadt, W. R.; Hay, P. J. *J. Chem. Phys.* **1985**, *82*, 284. Hay, P. J.; Wadt, W. R. *J. Chem. Phys.* **1985**, *82*, 299.
(31) Jacox, M. E.; Milligan, D. E. *J. Chem. Phys.* **1971**, *54*, 3935.
(32) Jacox, M. E.; Thompson, W. E. *J. Chem. Phys.* **1989**, *91*, 1410.
(33) Zhou, M. F.; Andrews, L. *J. Chem. Phys.* **1999**, *110*, 2414.
(34) Zhou, M. F.; Andrews, L. *J. Chem. Phys.* **1999**, *110*, 6820.
(35) Wang, X.; Zhou, M. F.; Andrews, L. *J. Phys. Chem. A* **2000**, *104*, 7964.
(36) Zhou, M. F.; Citra, A.; Liang, B.; Andrews, L. *J. Phys. Chem. A* **2000**, *104*, 3457.
(37) Allavena, M.; Rysnik, R.; White, D.; Calder, V.; Mann, D. E. *J. Chem. Phys.* **1969**, *50*, 3399.
(38) Andrews, L. *J. Electron Spectrosc. Relat. Phenom.* **1998**, *97*, 63.
(39) Zhou, M. F.; Andrews, L. *J. Am. Chem. Soc.* **1998**, *120*, 11499.
(40) Zhou, M. F.; Andrews, L. *J. Phys. Chem. A* **1999**, *103*, 7773.
(41) Liang, B.; Zhou, M. F.; Andrews, L. *J. Phys. Chem. A* **2000**, *104*, 3905.
(42) Liang, B.; Andrews, L. *J. Phys. Chem. A* **2002**, *106*, 595. (Re + CO_2).
(43) Zhou, M. F.; Andrews, L.; Bauschlicher, C. W., Jr. *Chem. Rev.* **2001**, *101*, 1931.